

# Finite-energy spin fluctuations as a pairing glue in systems with coexisting electron and hole bands

Masahiro Nakata,<sup>\*</sup> Daisuke Ogura, Hidetomo Usui, and Kazuhiko Kuroki<sup>†</sup>*Department of Physics, Osaka University, 1-1 Machikaneyama, Toyonaka, Osaka 560-0043, Japan*

(Received 2 May 2017; published 19 June 2017)

We study, within the fluctuation-exchange approximation, the spin-fluctuation-mediated superconductivity in Hubbard-type models possessing electron and hole bands, and compare them with a model on a square lattice with a large Fermi surface. In the large Fermi surface model, superconductivity is more enhanced for better nesting for a fixed band filling. By contrast, in the models with electron and hole bands, superconductivity is optimized when the Fermi surface nesting is degraded to some extent, where finite-energy spin fluctuations around the nesting vector develop. The difference lies in the robustness of the nesting vector, namely, in models with electron and hole bands, the wave vector at which the spin susceptibility is maximized is fixed even when the nesting is degraded, whereas when the Fermi surface is large, the nesting vector varies with the deformation of the Fermi surface. We also discuss the possibility of realizing in actual materials the bilayer Hubbard model, which is a simple model with electron and hole bands, and is expected to have a very high  $T_c$ .

DOI: [10.1103/PhysRevB.95.214509](https://doi.org/10.1103/PhysRevB.95.214509)

## I. INTRODUCTION

In the early days of the theoretical studies of the iron-based superconductors, the nesting between electron and hole Fermi surfaces was considered to be important for the occurrence of superconductivity. The intraorbital repulsion  $U$ , combined with the nesting, induces spin fluctuations, which in turn act as a repulsive pairing interaction around the nesting vector. A repulsive pairing interaction with a certain wave vector  $\mathbf{Q}$  generally tends to induce an unconventional superconducting gap, in which the sign changes across  $\mathbf{Q}$ . In the case of the iron-based superconductors, this mechanism leads to the so-called  $s\pm$ -wave pairing state, where the gap sign is reversed between the electron and the hole Fermi surfaces [1–6]. However, later experiments have suggested that high  $T_c$  is attained when the nesting is degraded, or even in the absence of the nesting [7–13]. In a previous study, two of the present authors pointed out that superconductivity can be enhanced even when the nesting is not good if the magnitude of the hopping integrals matches well the inverse Fourier transformation of the gap function from momentum space to real space [14]. The  $s\pm$ -wave pairing state corresponds to a next nearest neighbor pairing in real space, which goes hand-in-hand with the fact that the next nearest neighbor hopping is actually the dominant hopping in iron-based superconductors with high  $T_c$ . The importance of the real space picture implies that the states away from the Fermi level also play an important role, since the inverse Fourier transformation involves all the states within the Brillouin zone including the states away from the Fermi level. In fact, after the observation of missing hole Fermi surface in some of the iron-based superconductors [7–10,12,13,15], more focus has been paid on bands referred to as the “incipient band”, which lies below, but close to the Fermi level [1,12,16–19].

Given this background, here we analyze two Hubbard-type models with coexisting electron and hole bands within the fluctuation exchange (FLEX) approximation [20,21], and compare

them with the single band Hubbard model with a single large Fermi surface. We show that in models with electron and hole bands with a fixed band filling, superconductivity is optimized when the parameter values are such that the Fermi surface nesting is degraded to some extent. There, the finite-energy spin fluctuations, which originate from the states away from the Fermi level, develop and act as an effective pairing glue. This is in contrast to the case of the single band model, where better nesting gives higher  $T_c$  for a fixed band filling. Owing to this difference, in an ideal situation with electron and hole bands,  $T_c$  can be much higher than in the case with a single Fermi surface.

## II. THE MODELS

As an actual superconductor with electron and hole bands, we consider the iron-based superconductor. Although the calculation results do not qualitatively depend on the material we consider, we adopt the hydrogen doped LaFeAsO as a typical example, whose five orbital model was constructed in Ref. [14]. The electron doping rate taken here is 25%. As a simpler model possessing similar kinds of disconnected Fermi surfaces, we also consider a bilayer lattice system, where the bonding and the antibonding bands form electron and hole Fermi surfaces near half-filling (when the number of electrons is close to the number of sites) [22–32]. The model and its band structure are shown in Fig. 1. For this latter model, we fix the band filling at  $n = 0.9$ , where  $n = 1$  corresponds to half-filling.

In both of these systems, the nesting of the Fermi surface can be controlled by certain parameters for a fixed band filling. In the iron-based superconductor, the Fe-As-Fe bond angle  $\alpha$  controls the nesting of the Fermi surface originating from the  $d_{xy}$  orbital [33,35–37]. Namely, when the bond angle is large, the hole Fermi surface originating from the  $d_{xy}$  orbital around the Brillouin zone corner  $(\pi, \pi)$  is missing, but as the angle  $\alpha$  becomes smaller, the Fermi surface appears and grows larger, so that the nesting between the electron [centered around  $(\pi, 0)/(0, \pi)$ ] and the hole Fermi surfaces gets better. We refer to Fig. 1 of Ref. [14] for the variation of the Fermi surface with the change in the bond angle. In the bilayer model,

<sup>\*</sup>Present address: Mitsubishi Electric Corporation.<sup>†</sup>Corresponding author: kuroki@phys.sci.osaka-u.ac.jp

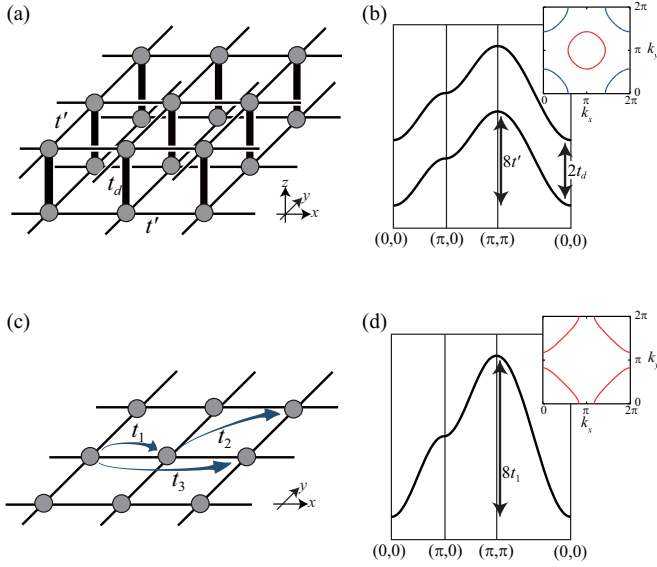


FIG. 1. (a) and (b) The bilayer model; (c) and (d) the single band model on a square lattice (the large-Fermi-surface model). (a) and (c) The lattice structure and the hoppings; (b) and (d) typical band structure and Fermi surface.

the ratio between the intralayer and the interlayer hoppings,  $t'$  and  $t_d$ , respectively, controls the Fermi surface nesting for non-half-filled cases. When  $t'/t_d$  is reduced, the overlap between the bonding and the antibonding bands becomes smaller to degrade the nesting, and eventually one of the Fermi surfaces disappears. Here  $t_d$  is fixed at 1.4 as in Ref. [27], and hence  $t_d/1.4$  is the unit of the energy.

As an example of systems with a large Fermi surface, we consider a single band Hubbard model on a square lattice, which is often considered as an effective model for the high  $T_c$  cuprates. As shown in Figs. 1(c) and 1(d), we consider hoppings up to third nearest neighbors  $t_1$  (fixed at  $-1$  here, so that  $|t_1|$  is the unit of the energy),  $t_2$ , and  $t_3$ , with  $t_2 = -t_3$  for simplicity (this relation is roughly satisfied in the cuprates). For a fixed band filling close to half-filling, the Fermi surface nesting becomes degraded when  $t_2 (= -t_3)$  is increased. For the single band model, we fix the band filling at  $n = 0.85$  (corresponds to 15% hole doping in the cuprates).

On top of these tight-binding models, we take into account the on-site electron-electron interactions, that is, the on-site Hubbard  $U$  for the bilayer and the large-Fermi-surface models, and the multiorbital interactions for the iron-based superconductor in the form

$$H_I = \sum_i \left[ \sum_{\mu} U_{\mu} n_{i\mu\uparrow} n_{i\mu\downarrow} + \sum_{\mu > \nu} \sum_{\sigma \sigma'} U'_{\mu\nu} n_{i\mu\sigma} n_{i\mu\sigma'} - \sum_{\mu \neq \nu} J_{\mu\nu} \mathbf{S}_{i\mu} \cdot \mathbf{S}_{i\nu} + \sum_{\mu \neq \nu} J'_{\mu\nu} c_{i\uparrow}^{\mu\dagger} c_{i\downarrow}^{\mu\dagger} c_{i\downarrow}^{\nu} c_{i\uparrow}^{\nu} \right]$$

in notations adopted in Ref. [33]. We apply the FLEX approximation to obtain the renormalized Green's function, the spin and charge susceptibilities, which are plugged into the Eliashberg equation to study superconductivity. The values of the electron-electron interactions for the model of the

iron-based superconductor are  $U = 1.3$  eV,  $U' = 2U/3$ , and  $J = J' = U/6$ .  $U = 6$  and  $U = 8$  for the large-Fermi surface and the bilayer model, respectively, in units adopted in each model. The temperature is  $T = 0.01$  eV for the model of the iron-based superconductor, and  $T = 0.1$  and  $T = 0.03$  for the bilayer and the large-Fermi-surface model in units taken for each model. The number of  $k$ -point meshes is  $32 \times 32$  for the large-Fermi-surface model, and  $64 \times 64$  for the iron-based superconductor and the bilayer model. The number of Matsubara frequencies is 2048 for the large-Fermi-surface model and the iron-based superconductor, and 4096 for the bilayer. For the model of the iron-based superconductor, as was done in Ref. [34], we subtract the  $\omega = 0$  component of the self-energy for each FLEX iteration, which is considered to be taken into account already in the first-principles band calculation.

We focus on the imaginary part of the dynamical spin susceptibility  $\chi(\mathbf{q}, \omega)$ , which is experimentally observed in NMR and neutron scattering experiments as a measure for the strength of the spin fluctuations in momentum and energy space.  $\chi(\mathbf{q}, \omega)$  is obtained by Padé analytical continuation of the FLEX spin susceptibility obtained within the Matsubara formalism. For the model of the iron-based superconductor, we obtain the susceptibility in the orbital representation and take the diagonal element  $\chi^{\mu\mu\mu\mu}(\mathbf{q}, i\omega)$  ( $\mu$  denotes the orbitals; see Ref. [33]) with  $\mu = d_{xy}$  orbital. The reason for taking only the  $d_{xy}$  component is because (i) our previous study [14] has shown that superconductivity is mainly governed by the  $d_{xy}$  orbital for the doping rate larger than 15% (here the doping rate is 25%), and (ii) the bond angle controls the presence/absence of the  $d_{xy}$  orbital portion of the Fermi surface around  $(\pi, \pi)$  as mentioned earlier in Sec. II. As for the bilayer model,  $\chi$  is a  $2 \times 2$  matrix [27], and we take the trace of this matrix as  $\chi(\mathbf{q}, i\omega)$ . As a quantity that measures the strength of the spin fluctuations, we define  $\text{Im } \Gamma(\omega)$  as

$$\sum_{\mathbf{q}} \text{Im } \chi(\mathbf{q}, \omega) \equiv \text{Im } \Gamma(\omega). \quad (1)$$

The dominant contribution in this summation comes from around certain wave vectors (the nesting vector in a broad sense of the term)  $\mathbf{Q}$ , where  $\mathbf{Q} = (\pi, \pi)$  for the bilayer and large-Fermi-surface models (see Fig. 1), and  $\mathbf{Q} = (\pi, 0)$  for the iron-based superconductor [the nesting is between the hole Fermi surface around  $(\pi, \pi)$  and the electron Fermi surfaces around  $(\pi, 0)/(0, \pi)$ , see, e.g., Fig. 1 of Ref. [14]]. For the model of the iron-based superconductor, we find that the  $\text{Im } \chi[\mathbf{q} \simeq (0, 0), \omega]$  also exhibits some bond angle dependence. Since this is related neither to the Fermi surface nesting nor the  $\pm$ -wave pairing glue, we restrict the summation to the area of  $(1/8)^2$  of the Brillouin zone around  $\mathbf{Q}$ . As for superconductivity, the Green's function is plugged into the linearized Eliashberg equation, whose eigenvalue  $\lambda$  reaches unity at  $T = T_c$  of superconductivity. Here we calculate  $\lambda$  at a fixed temperature for each system to measure how close the system is to the superconducting transition.

### III. RESULTS

We start with the iron-based superconductors. In Fig. 2(a), we plot  $\text{Im } \Gamma(\omega)$  as functions of  $\omega$  for various hypothetical

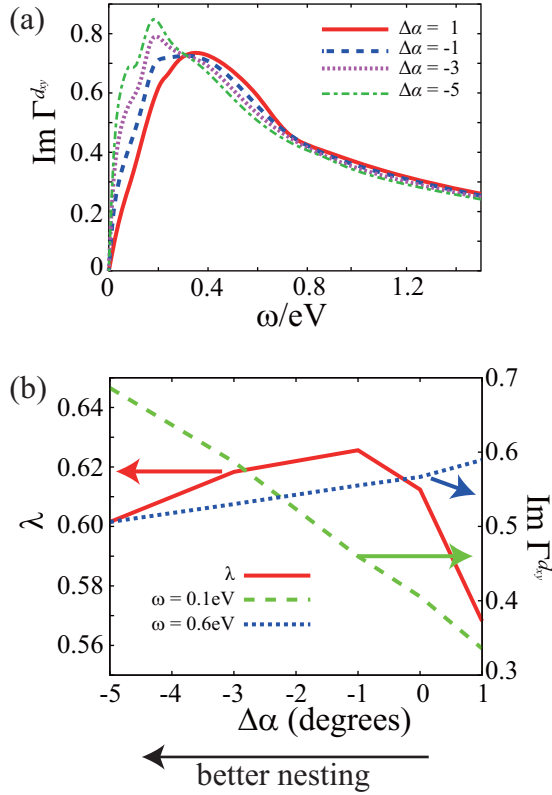


FIG. 2. FLEX calculation result for the five orbital model of the iron-based superconductor. (a)  $\text{Im } \Gamma^{d_{xy}}$  as functions of  $\omega$  for various bond angles. (b) Eigenvalue of the  $s_{\pm}$  superconducting state (left axis) and  $\text{Im } \Gamma^{d_{xy}}$  (right axis) for low and high  $\omega$  values, plotted against the bond angle.

values of the Fe-As-Fe bond angle. Here, the bond angle is presented as the deviation  $\Delta\alpha$  (degrees) from the bond angle of  $\text{LaFeAsO}_{0.75}\text{H}_{0.25}$  observed experimentally [14]. (The hypothetical variation of  $\alpha$  corresponds to substituting La and/or As with other elements). When the bond angle is small and hence the Fermi surface nesting is good, the spin fluctuations around the wave vector  $(\pi, 0)/(0, \pi)$  are large in the small  $\omega$  regime, but when the bond angle becomes large and the nesting is degraded, the low-energy spin fluctuations lose weight, and the fluctuation weight moves towards higher energy regime. In Fig. 2(b), the eigenvalue of the Eliashberg equation is plotted as a function of the Fe-As-Fe bond angle, along with the value of  $\text{Im } \Gamma$  at certain high and low energies. As already expected from Fig. 2(a), the high- and low-energy spin fluctuations have the opposite tendency with respect to the Fermi surface nesting. Superconductivity is optimized at a certain bond angle, which can be considered as a consequence of the spin fluctuations lying in a finite “sweet spot” energy regime for superconductivity. In other words, superconductivity is optimized for moderate Fermi surface nesting, and neither too good nor too ill-conditioned nesting is favorable for superconductivity. Since  $\lambda$  is positively correlated with  $T_c$ , the present result explains the experimental observation that there is an optimal Fe-As-Fe bond angle for the iron-based superconductors [38]. Also, as was pointed out by two of the present authors in Ref. [39], the above

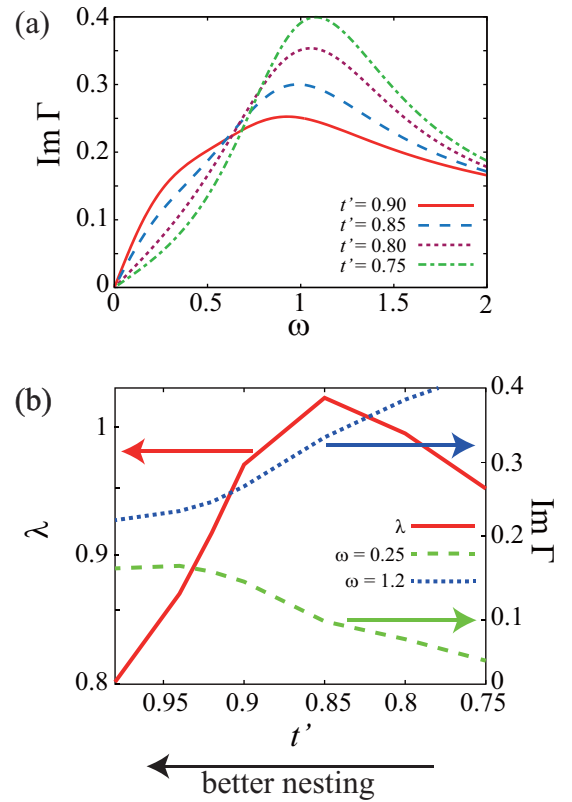


FIG. 3. Plots similar to Fig. 2 for the bilayer model. Here, the parameter that controls the nesting is the intralayer hopping  $t'$ .

picture explains the experimental (NMR) observation found in some of the iron-based superconductors that the strength of the low-energy spin fluctuations is not positively correlated with  $T_c$  [40–42].

In Fig. 3, we present similar calculation results for the bilayer model. When  $t'$  is small so that the Fermi surface nesting is good, the spin fluctuations have large weight in the low-energy regime, whereas when  $t'$  is large and the nesting is degraded, the spin fluctuation weight moves towards higher energy regime. Consequently, superconductivity is optimized at a certain  $t'$  that gives moderate nesting. These results suggest that the two models with disconnected Fermi surfaces share a common feature: Superconductivity is optimized for somewhat degraded Fermi surface nesting, for which the spin fluctuations around the nesting vector have large weight in a finite sweet spot energy regime for superconductivity [43].

We now move on to the single band model on a square lattice, i.e., the large-Fermi-surface model, for comparison. In this case, the spin fluctuations around the wave vector  $(\pi, \pi)$  are monotonically reduced in the entire energy range as  $t_2 (= -t_3)$  is increased to degrade the Fermi surface nesting, as shown in Fig. 4(a). Consequently, the eigenvalue of the  $d$ -wave superconductivity monotonically decreases with increasing  $t_2$  [44]. This is in sharp contrast to the cases when the Fermi surface consists of disconnected pockets.

#### IV. DISCUSSION

The origin of the above results can be understood as follows. In the case of systems with disconnected Fermi

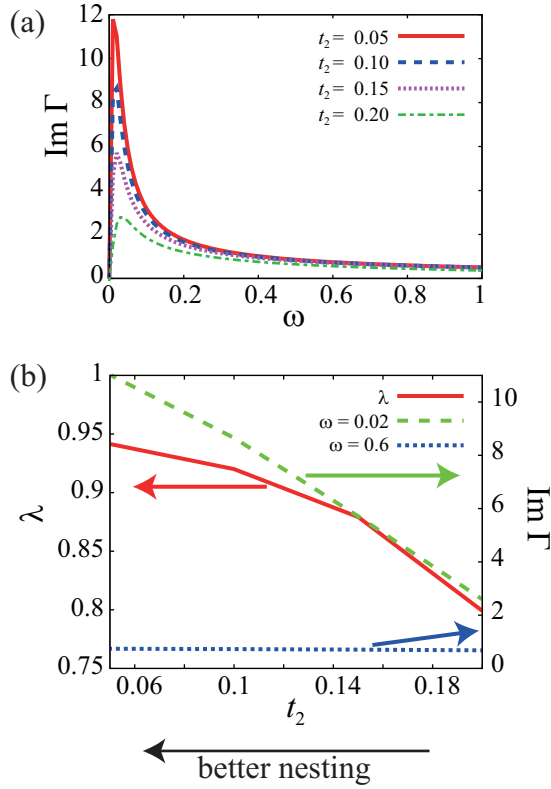


FIG. 4. Plots similar to Fig. 2 for the single band model on a square lattice (the large-Fermi-surface model). Here, the parameter that controls the nesting is the distant hoppings  $t_2 = (-t_3)$ .

surfaces, the nesting vector, i.e., the wave vector where the spin susceptibility is maximized, is basically unchanged from its original position  $[(\pi, \pi)$  for the bilayer model and  $(\pi, 0)/(0, \pi)$  for the iron-based superconductor] even when the nesting is degraded. This is because the Fermi surface is small so that there are no other candidates for the nesting vector (to be precise, this is not completely correct for the iron-based superconductor; we will come back to this point later). On the other hand, when the Fermi surface is large as in the present single band model, there will appear other candidates for the nesting vector when the shape of the Fermi surface is deformed. Therefore, the weight of the spin fluctuations will be spread and transferred to various wave vector positions. This is unfavorable for  $d$ -wave superconductivity since its gap function has to change its sign across the wave vector at which the spin fluctuations are maximized; if a wave vector at which the spin fluctuations have significant weight connects the portion of the Fermi surface with the same sign of the superconducting gap, that will give a negative contribution to superconductivity.

In the case of the disconnected Fermi surfaces, the weight of the spin fluctuations is transferred mainly in the energy direction without basically changing the wave vector when the nesting is degraded, so that there is a large potential of the optimized  $T_c$  being higher than in the case with a large Fermi surface. In fact, previous studies have shown that the bilayer model exhibits extremely high  $T_c$  compared to the single band Hubbard model [27,32]. This is also reproduced

in the present study, as seen in Fig. 3(b), where the eigenvalue of the Eliashberg equation  $\lambda$  exceeds unity at  $t' = 0.85$  and  $T = 0.1$ , meaning that  $T_c$  is larger than  $0.1t'$ . This  $T_c$  is more than three times higher than that ( $\sim 0.03t$ ) of the single band model [45]. It is also worth noting that the high  $T_c$  in the bilayer model is realized despite the fact that the spin fluctuations are not so strong, as seen by comparing the absolute value of  $\text{Im}\Gamma$  [Fig. 3(a)] to that of the single band model [Fig. 4(a)]. This implies that the high  $T_c$  superconductivity in the bilayer model can take place without closely competing with magnetism, once the appropriate parameter values are realized.

$T_c$  of the bilayer model is also much higher than that of the model of the iron-based superconductors, although the latter also has disconnected Fermi surfaces [45]. There are actually two reasons for this. (i) The multiorbital nature degrades the effect of the spin-fluctuation-mediated pairing glue; the spin fluctuations can be most effective as a pairing glue when only one up- and one down-spin electrons can occupy the same site, that is, in the case of single orbital systems. (ii) When the bond angle becomes so large that the  $d_{xy}$  Fermi surface around  $(\pi, \pi)$  is completely lost, spin fluctuations develop around another nesting vector  $(\pi/2, \pi)/(\pi, \pi/2)$  between the two electron Fermi surfaces [33,46]. Therefore, the nesting vector is not as robust as in the bilayer model.

The bilayer model is, at present, a toy model which does not correspond to an actual material, but the above discussion suggests that if a corresponding material is found, it may have  $T_c$  even higher than that of the cuprate superconductors. It is thus tempting to search for materials that actually correspond to the present bilayer model. An important feature of this model is that the interlayer hopping  $t_d$  is moderately (about two times) larger than the intralayer one  $t'$ . Hence, candidates may be found in materials with nearly half-filled  $d_{3z^2-r^2}$  orbital, rather than the  $d_{x^2-y^2}$  orbital that plays the main role in the cuprates. As a possible candidate toward this direction, we focus on a particular existing Ruddlesden-Poppers compound,  $\text{La}_3\text{Ni}_2\text{O}_7$ , which has a bilayer structure of  $\text{NiO}_2$  planes. The  $3d^{7.5}$  configuration in the nickelate, rather than the  $3d^9$  in the cuprates, makes the  $d_{3z^2-r^2}$  band close to half filling. The material is nonsuperconducting, and previous studies have suggested that the  $d_{3z^2-r^2}$  orbital is in the half-filled Mott insulating state, while the overlapping quarterfilled band originating from the  $d_{x^2-y^2}$  orbital is metallic [47]. Nonetheless, we perform a band calculation [48] to see whether a band structure similar to that of the bilayer model could emerge, were it not for the Mott insulating state. We carry out the band calculation using the WIEN2K package [50], assuming an ideal, undistorted lattice structure and a paramagnetic phase, and adopting the experimentally determined lattice structure [49]. We set  $RK_{\text{max}} = 6.5$  and employ 512  $k$  meshes.

The obtained band structure is shown in Fig. 5. If we focus on the bands originating from the  $d_{3z^2-r^2}$  orbital, we can see that there indeed exist bonding and antibonding bands, similar to those of the bilayer model. However, the overlap between the two bands is barely present, meaning that  $t_d$  is about  $4t'$  (see Fig. 1), which is somewhat large from the viewpoint of the present calculation results. If the layer-layer distance can somehow be enlarged (and, of course, the orbital selective Mott insulating state of the  $d_{3z^2-r^2}$  orbital can be circumvented), the situation will be closer to that of the bilayer model. Another



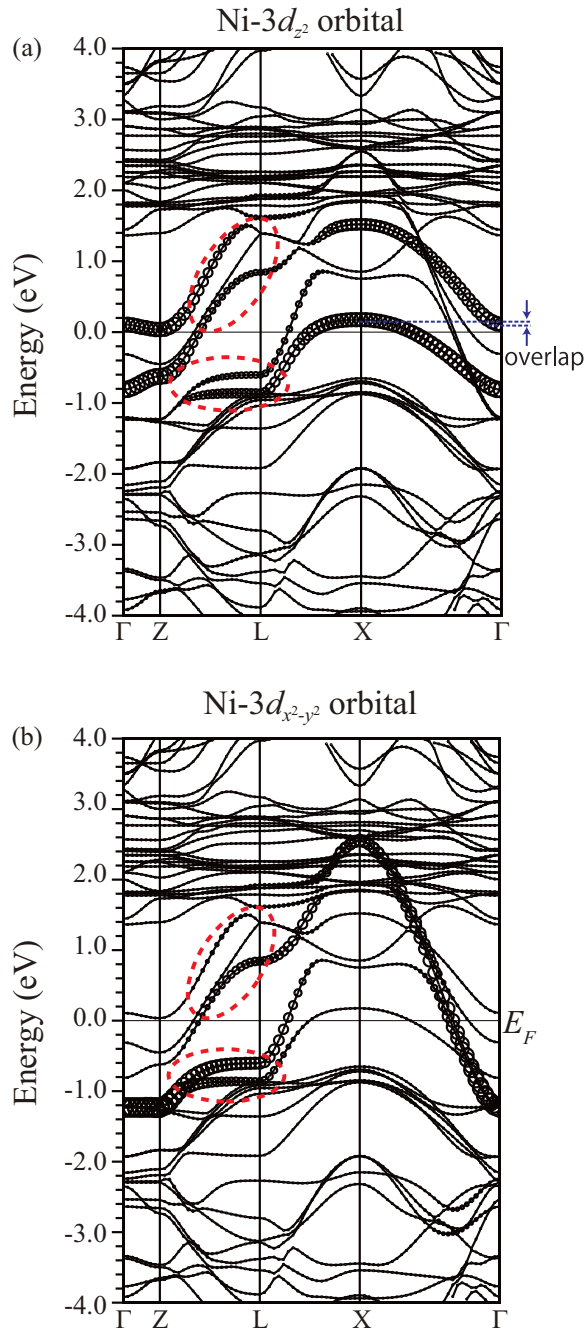


FIG. 5. Band calculation result for  $\text{La}_3\text{Ni}_2\text{O}_7$ . The thickness of the lines in (a) depict the  $d_{3z^2-r^2}$  weight, and in (b) the  $d_{x^2-y^2}$  weight. The  $d_{3z^2-r^2}$  and the  $d_{x^2-y^2}$  orbitals strongly hybridize in the portion encircled by the dashed line.

point that should be noticed is the  $d_{x^2-y^2}$  orbital contribution; the  $d_{x^2-y^2}$  band strongly overlaps with the  $d_{3z^2-r^2}$  band, and

there is a  $d_{3z^2-r^2}$ - $d_{x^2-y^2}$  hybridization around the portion encircled by the dashed lines, which deforms the  $d_{3z^2-r^2}$  band from the ideal shape shown in Fig. 1. This hybridization may degrade superconductivity, as was shown in the case of the cuprates; there, the situation is the opposite, namely, the main band is the  $d_{x^2-y^2}$  band, and the hybridization with the  $d_{3z^2-r^2}$  orbital degrades the superconductivity [51,52]. In the present case, the  $d_{x^2-y^2}$  band may have to be lifted to higher energies, using, e.g., certain modification of the crystal field, to reduce the hybridization effect. Further study along this line is in progress.

## V. CONCLUSION

We have studied the spin-fluctuation-mediated superconductivity in Hubbard-type models possessing electron and hole bands, and compared them with the Hubbard model on a square lattice with a large Fermi surface. In the former models, superconductivity is optimized when the Fermi surface nesting is degraded to some extent, and finite-energy spin fluctuations around the nesting vector develops. This is in contrast to the case of the large-Fermi-surface model, where superconductivity is more enhanced for better nesting. The difference lies in the robustness of the nesting vector, namely, in models with electron and hole bands, the wave vector at which the spin susceptibility is maximized is fixed even when the nesting is degraded, whereas when the Fermi surface is large, the nesting vector varies with the deformation of the Fermi surface.

As seen in the calculation result for the bilayer model, the large enhancement of the finite-energy spin fluctuations around the robust nesting vector can give rise to an extremely high  $T_c$ , although such a situation is realized only in a narrow “sweet spot” regime in the parameter space. Our band calculation result shows that such a situation might be realized by modifying the lattice structure and the constituting elements of existing bilayer materials.

## ACKNOWLEDGMENTS

We thank Hiroshi Eisaki for pointing out the possible relevance of  $\text{La}_3\text{Ni}_2\text{O}_7$  to the bilayer model. We also thank Hideo Aoki and Kenji Kawashima for discussions on the realization of the bilayer model in actual materials. We also appreciate Katsuhiko Suzuki for the assistance with the multiorbital FLEX code. Part of the calculation was performed using supercomputers at the Supercomputer Center, Institute for Solid State Physics, The University of Tokyo. This study was supported by Grants-in-Aid for Scientific Research (A) (Grant No. JP26247057) and Grants-in-Aid for Scientific Research (B) (Grant No. JP16H04338) from the Japan Society for the Promotion of Science. D.O. acknowledges support from Grant-in-Aid for JSPS Research Fellow Grant No. 16J01021.

- [1] P. J. Hirschfeld, M. M. Korshunov, and I. I. Mazin, *Rep. Prog. Phys.* **74**, 124508 (2011).
- [2] K. Kuroki, in *Iron-based Superconductors: Materials, Properties and Mechanisms* (Pan Stanford Publishing, Singapore, 2013), Chap. 8.

- [3] A. Chubukov and P. J. Hirschfeld, *Phys. Today* **68**, 46 (2015).
- [4] H. Hosono and K. Kuroki, *Physica C (Amsterdam)* **514**, 399 (2015).
- [5] I. I. Mazin, D. J. Singh, M. D. Johannes, and M. H. Du, *Phys. Rev. Lett.* **101**, 057003 (2008).

- [6] K. Kuroki, S. Onari, R. Arita, H. Usui, Y. Tanaka, H. Kontani, and H. Aoki, *Phys. Rev. Lett.* **101**, 087004 (2008).
- [7] J. Guo, S. Jin, G. Wang, S. Wang, K. Zhu, T. Zhou, M. He, and X. Chen, *Phys. Rev. B* **82**, 180520 (2010).
- [8] T. Qian, X.-P. Wang, W.-C. Jin, P. Zhang, P. Richard, G. Xu, X. Dai, Z. Fang, J.-G. Guo, X.-L. Chen, and H. Ding, *Phys. Rev. Lett.* **106**, 187001 (2011).
- [9] Q. Y. Wang *et al.*, *Chin. Phys. Lett.* **29**, 037402 (2012).
- [10] S. Tan *et al.*, *Nat. Mater.* **12**, 634 (2013).
- [11] S. Iimura, S. Matsuishi, H. Sato, T. Hanna, Y. Muraba, S. W. Kim, J. E. Kim, M. Takata, and H. Hosono, *Nat. Commun.* **3**, 943 (2012).
- [12] H. Miao, T. Qian, X. Shi, P. Richard, T. K. Kim, M. Hoesch, L. Y. Xing, X.-C. Wang, C.-Q. Jin, J.-P. Hu, and H. Ding, *Nat. Commun.* **6**, 6056 (2015).
- [13] X. H. Niu, R. Peng, H. C. Xu, Y. J. Yan, J. Jiang, D. F. Xu, T. L. Yu, Q. Song, Z. C. Huang, Y. X. Wang, B. P. Xie, X. F. Lu, N. Z. Wang, X. H. Chen, Z. Sun, and D. L. Feng, *Phys. Rev. B* **92**, 060504 (2015).
- [14] K. Suzuki, H. Usui, S. Iimura, Y. Sato, S. Matsuishi, H. Hosono, and K. Kuroki, *Phys. Rev. Lett.* **113**, 027002 (2014).
- [15] The complete absence of the hole Fermi surface in  $K_x\text{Fe}_{2-y}\text{Se}_2$  is still controversial; in fact, a recent ARPES study [Sunagawa *et al.*, *J. Phys. Soc. Jpn.* **85**, 073704 (2016)] observes a “hidden” hole band, which was detected by taking special care of the photon energy and the polarization, likely to be intersecting the Fermi level.
- [16] F. Wang, F. Yang, M. Gao, Z.-Y. Lu, T. Xiang, and D.-H. Lee, *Europhys. Lett.* **93**, 57003 (2011).
- [17] Y. Bang, *New J. Phys.* **16**, 023029 (2014).
- [18] X. Chen, S. Maiti, A. Linscheid, and P. J. Hirschfeld, *Phys. Rev. B* **92**, 224514 (2015).
- [19] Y. Bang, *New J. Phys.* **18**, 113054 (2016).
- [20] N. E. Bickers, D. J. Scalapino, and S. R. White, *Phys. Rev. Lett.* **62**, 961 (1989).
- [21] T. Dahm and L. Tewordt, *Phys. Rev. Lett.* **74**, 793 (1995).
- [22] N. Bulut, D. J. Scalapino, and R. T. Scalettar, *Phys. Rev. B* **45**, 5577 (1992).
- [23] R. T. Scalettar, J. W. Cannon, D. J. Scalapino, and R. L. Sugar, *Phys. Rev. B* **50**, 13419 (1994).
- [24] R. E. Hetzel, W. von der Linden, and W. Hanke, *Phys. Rev. B* **50**, 4159 (1994).
- [25] R. R. dos Santos, *Phys. Rev. B* **51**, 15540 (1995).
- [26] A. I. Liechtenstein, I. I. Mazin, and O. K. Andersen, *Phys. Rev. Lett.* **74**, 2303 (1995).
- [27] K. Kuroki, T. Kimura, and R. Arita, *Phys. Rev. B* **66**, 184508 (2002).
- [28] S. S. Kancharla and S. Okamoto, *Phys. Rev. B* **75**, 193103 (2007).
- [29] K. Bouadim, G. G. Batrouni, F. Hébert, and R. T. Scalettar, *Phys. Rev. B* **77**, 144527 (2008).
- [30] N. Lanata, P. Barone, and M. Fabrizio, *Phys. Rev. B* **80**, 224524 (2009).
- [31] H. Zhai, F. Wang, and D.-H. Lee, *Phys. Rev. B* **80**, 064517 (2009).
- [32] T. A. Maier and D. J. Scalapino, *Phys. Rev. B* **84**, 180513(R) (2011).
- [33] K. Kuroki, H. Usui, S. Onari, R. Arita, and H. Aoki, *Phys. Rev. B* **79**, 224511 (2009).
- [34] H. Ikeda, R. Arita, and J. Kuneš, *Phys. Rev. B* **81**, 054502 (2010).
- [35] T. Miyake, T. Kosugi, S. Ishibashi, and K. Terakura, *J. Phys. Soc. Jpn.* **79**, 123713 (2010).
- [36] H. Usui and K. Kuroki, *Phys. Rev. B* **84**, 024505 (2011).
- [37] O. K. Andersen and L. Boeri, *Ann. Phys. (Berlin)* **523**, 8 (2011).
- [38] C. H. Lee, A. Iyo, H. Eisaki, H. Kito, M. T. Fernandez-Diaz, T. Ito, K. Kihou, H. Matsuhata, M. Braden, and K. Yamada, *J. Phys. Soc. Jpn.* **77**, 083704 (2008).
- [39] H. Arai, H. Usui, K. Suzuki, Y. Fuseya, and K. Kuroki, *Phys. Rev. B* **91**, 134511 (2015).
- [40] K. Ishida, Y. Nakai, and H. Hosono, *J. Phys. Soc. Jpn.* **78**, 062001 (2009).
- [41] H. Mukuda, F. Engetsu, K. Yamamoto, K. T. Lai, M. Yashima, Y. Kitaoka, A. Takemori, S. Miyasaka, and S. Tajima, *Phys. Rev. B* **89**, 064511 (2014).
- [42] T. Shiotani, H. Mukuda, M. Uekubo, F. Engetsu, M. Yashima, Y. Kitaoka, K. T. Lai, H. Usui, K. Kuroki, S. Miyasaka, and S. Tajima, *J. Phys. Soc. Jpn.* **85**, 053706 (2016).
- [43] For the parameter values that optimize superconductivity in these systems, the hole and the electron Fermi surfaces both exist in the noninteracting band structure, i.e., the band structure for  $U = 0$ . However, in the actual renormalized band structure, the presence/absence of one of the Fermi surfaces becomes a subtle problem, as can be roughly seen from the FLEX calculation result of the dressed Green function at the lowest Matsubara frequency. Here we will not go into this problem since a precise evaluation requires highly accurate analytical continuation.
- [44] This is actually opposite to the tendency found for the cuprate superconductors [E. Pavarini, I. Dasgupta, T. Saha-Dasgupta, O. Jepsen, and O. K. Andersen, *Phys. Rev. Lett.* **87**, 047003 (2001)]. It was revealed in Refs. [51,52] that this contradiction is due to an oversimplification of the single band model, where the effect of the  $d_{3z^2-r^2}$  orbital is taken into account only implicitly.
- [45] Although we take somewhat different values of  $U$  between the bilayer and the large-Fermi-surface models, this does not affect the conclusion here since  $T_c$  is not strongly dependent on the value of  $U$  around these values. Also, the intraorbital  $U = 1.3$  eV of the model of the iron-based model is of the same order with those in other models when measured in units of a typical hopping integral in the iron-based superconductors, i.e., order of 0.1 eV. A similar comment applies also to the difference in the doping rate among the three models.
- [46] S. Graser, T. A. Maier, P. J. Hirschfeld, and D. J. Scalapino, *New J. Phys.* **11**, 025016 (2009).
- [47] Y. Kobayashi, S. Taniguchi, M. Kasai, M. Sato, T. Nishioka, and M. Kontani, *J. Phys. Soc. Jpn.* **65**, 3978 (1996).
- [48] Band calculation for  $\text{La}_3\text{Ni}_2\text{O}_{7-\delta}$  has been performed for various oxygen deficiency rate as well as lattice structure distortion in work by V. Pardo and W. E. Pickett, *Phys. Rev. B* **83**, 245128 (2011).
- [49] Z. Zhang, M. Greenblatt, and J. B. Goodenough, *J. Solid State Chem.* **108**, 402 (1994).
- [50] P. Blaha, K. Schwarz, G. K. H. Madsen, D. Kvasnicka, and J. Luitz, *WIEN2k, An Augmented Plane Wave + Local Orbitals Program for Calculating Crystal Properties* (Karlheinz Schwarz, Techn. Universität Wien, Austria, 2001).
- [51] H. Sakakibara, H. Usui, K. Kuroki, R. Arita, and H. Aoki, *Phys. Rev. Lett.* **105**, 057003 (2010).
- [52] H. Sakakibara, H. Usui, K. Kuroki, R. Arita, and H. Aoki, *Phys. Rev. B* **85**, 064501 (2012).